Sliding-Mode Control of Neutral-Point-Clamped Power Converters With Gain Adaptation

Xiaoning Shen, *Member, IEEE*, Jianxing Liu, *Senior Member, IEEE*, Zhuang Liu, *Graduate Student Member, IEEE*, Yabin Gao, *Member, IEEE*, Jose I. Leon, *Fellow, IEEE*, Sergio Vazquez, *Fellow, IEEE*, Ligang Wu, *Fellow, IEEE*, and Leopoldo G. Franquelo, *Life Fellow, IEEE*

***Abstract*—Both the proportional-integral (PI) controller and the super-twisting algorithm (STA) are attractive alternatives to effectively govern power converters. The PI controller is smooth but is less robust to disturbances, while the STA exhibits good robustness with respect to disturbances but suffers from the negative effect of chattering when some high control gains are required in actual applications. To combine the advantages of both controllers, this article explores a novel observer-based varying exponent gain STA control scheme for the three-level neutral-point-clamped converter. By introducing a time-varying exponent gain into the STA, the proposed novel varying exponent gain STA combines the attractive traits of the PI controller (smooth control input) and the STA (robustness and fast dynamic response) simultaneously. In this sense, the controller exhibits a high performance in steady state as well as transient and provides strong robustness with respect to disturbances. In addition to the new controller, a higher order sliding-mode observer is integrated into the control scheme to compensate the disturbances and further enhance the disturbances rejection ability of the system. Finally, the effectiveness of the proposed control method is confirmed by comparing its results with the PI controller and the STA based on a set of experiments.**

***Index Terms*—Gain adaptation, neutral-point-clamped (NPC) converter, observer design, sliding-mode control.**

Manuscript received 17 September 2023; revised 20 January 2024; accepted 31 March 2024. Date of publication 9 April 2024; date of current version 20 June 2024. This work was supported in part by the National Natural Science Foundation of China under Grant 62373127, Grant 62033005, and Grant 62320106001, in part by the Fundamental Research Funds for the Central Universities under Grant HIT.OCEF. 2024004, in part by the Natural Science Foundation of Heilongjiang Province under Grant ZD2021F001, in part by the State Key Laboratory of Alternate Electrical Power System with Renewable Energy Sources under Grant LAPS23005, in part by the Foundation of The International Science and Technology Cooperation Center of Renewable Energy and HybridPower, Shaanxi, under Grant HK-YF-FY-20231011004, in part by the postdoctoral initial funding of Heilongjiang Province under Grant LBH-Q21016 and Grant LBH-Q21097, in part by the Self-Planned Task (SKLRS202215B) of State Key Laboratory of Robotics and System (HIT), in part by the Key R&D Program of Heilongjiang Province under Grant 2022ZX01A18, in part by the China Postdoctoral Science Foundation under Grant 2022M720960, and in part by the Heilongjiang Postdoctoral Fund under Grant LBH-Z22119. Recommended for publication by Associate Editor S. Ali Khajehoddin. *(Corresponding author: Jianxing Liu.)*

Xiaoning Shen, Jianxing Liu, Zhuang Liu, Yabin Gao, and Ligang Wu are with the Department of Control Science and Engineering, Harbin Institute of Technology, Harbin 150000, China (e-mail: xn_shen@hit.edu.cn; jx.liu@hit.edu.cn; liuz@hit.edu.cn; yabingao@hit.edu.cn; ligangwu@hit.edu.cn).

Jose I. Leon and Leopoldo G. Franquelo are with the ENGREEN Laboratory of Engineering for Energy and Environmental Sustainability, Universidad de Sevilla, 41092 Sevilla, Spain, and also with the School of Astronautics, Harbin Institute of Technology, Harbin 150001, China (e-mail: jileon@us.es; lgfranquelo@ieee.org).

Sergio Vazquez is with the Department of Electronic Engineering, Universidad de Sevilla, 41004 Sevilla, Spain (e-mail: sergi@us.es).

Color versions of one or more figures in this article are available at https://doi.org/10.1109/TPEL.2024.3386800.

Digital Object Identifier 10.1109/TPEL.2024.3386800

Nomenclature

v_{abc}	$[v_a, v_b, v_c]^T$, ac voltage based on abc-axis.
i_{abc}	$[i_a, i_b, i_c]^T$, ac current based on abc-axis.
δ_{abc}	$[\delta_a, \delta_b, \delta_c]^T$, average duty cycles in abc-axis.
$v_{\alpha\beta}$	$[v_\alpha, v_\beta]^T$, ac voltage based on $\alpha\beta\gamma$-axis.
$i_{\alpha\beta}$	$[i_\alpha, i_\beta]^T$, ac current based on $\alpha\beta\gamma$-axis.
$\delta_{\alpha\beta}$	$[\delta_\alpha, \delta_\beta]^T$, average duty cycles in $\alpha\beta\gamma$-axis.
$v_{\rm dc1}$, $v_{\rm dc2}$	Capacitors voltages of the dc link.
$v_{\rm dc}$	$(v_{\rm dc1} + v_{\rm dc2})$, dc-link voltage.
$e_{\rm dc}$	$(v_{\rm dc1} - v_{\rm dc2})$, error between capacitors voltages.
p, p^*	Active power, the reference of active power.
q, q^*	Reactive power, the reference of reactive power.
L, C, $R_{\rm dc}$	Line inductor, dc-link capacitor, and dc load.
ω	Frequency of ac voltage.

I. Introduction

With the increase of the power ratings in industrial systems, the three-level neutral-point-clamped (NPC) active front-end (AFE) converter has emerged as an attractive alternative for a wide range of medium-voltage applications, which can be found in motor drives [1], dc microgrids [2], and a variety of renewable energy sources (RESs) [3].

In spite of the growing application of the NPC AFE converter, the control of this topology still remains a challenge. Generally, the conventional proportional-integral (PI) controller is a good choice to manage such converter thanks to its simplicity in implementation. It provides smooth control input and has been widely used in a variety of industrial applications [4]. However, in actual applications, this converter might be subject to various disturbances, e.g., the load step in motor drive application, or the active power impact generated by RESs, which may give rise to the fluctuation of dc-link voltage. It is difficult to solve this problem with a conventional PI method since this approach is less robust to disturbances, and the performance of PI controller is degraded in the presence of perturbations/uncertainties [5]. This fact makes the nonlinear control receive increasing attention in the power electronic area, and a good number of nonlinear algorithms have been proposed for the power converters in the last few years [6], such as sliding-mode control [7], [8], [9], model predictive control [10], and intelligent control [11]. Model

predictive control can deal with multivariable and nonlinear cases in an intuitive way, however, this method requires an accurate model of the power converter [12]. Intelligent control does not depend on the mathematical model of the system. However, the design and implementation process of this method is complex, which limits its application to power converters. Compared with them, sliding-mode control is easy to implement and presents enhanced robustness against model uncertainties, which has become an attractive solution in handling perturbations/uncertainties of nonlinear systems.

Over the past few years, a variety of sliding-mode controllers have been proposed and developed in the literature, such as higher order sliding-mode controllers [13], terminal sliding-mode controllers [14], and fractional-order sliding-mode controllers [15]. Among them, terminal sliding-mode control features fast response and finite-time convergence. However, this method has a singularity problem. Fractional-order sliding-mode control inherits the advantages of integer-order sliding-mode control, but the computational processes of fractional-order differentiation are complicated. Higher order sliding-mode controllers, such as second-order twisting algorithm and third-order sliding-mode algorithm, generally require the information of higher order derivatives of sliding-mode variables, which is not easy to obtain in power electronic systems. Compared with them, the well-known second-order super-twisting algorithm (STA) only requires the information of sliding variables and offers appealing characteristics, such as fast dynamic response, robustness regarding perturbations/uncertainties, and simple computational procedures, which is an attractive solution for power converters. In [16], an observer-based STA control method is proposed to enhance the performance of NPC converter. In [17], the STA is utilized to regulate the dc-link voltage and the instantaneous power of NPC converter. And in [18], a super-twisting differentiator-based STA method is proposed to regulate the current of two-level power converter under unbalanced grid condition. However, although STA is an attractive alternative to assure robustness regarding perturbations/uncertainties and fast trajectory tracking, the high-frequency switching motion (the so-called chattering phenomenon) could be exacerbated if some high control gains are used in actual applications.

An alternative to attenuate the chattering is the adaptive-gain STA approaches [19], [20], [21]. The core idea of these works is using time-varying gains to adapt the unknown perturbations without overestimating the control gains. However, these control schemes generally require numerous control parameters, which complicates both tuning and physical implementation.

Recently, a solution to attenuate the chattering and maintain the robustness of the sliding-mode control with the idea of using varying exponent gain α was proposed in [22], [23], [24], and [25]. The first work to present this idea is [22], in which the proposed control algorithm switches between the second-order linear state feedback control and the twisting control by adjusting the exponent gain α between 1 and 0. In this way, this method captures the advantages of both controllers. In [23], this controller is applied to an electropneumatic actuator. Afterwards, to assure a smooth switching between the two controllers, in [24], a dynamically adapted exponent gain α varying between 1 and 0 is used instead of an abrupt switching. In [25], besides the second-order controller, the first-order controller with a varying exponent gain α is also investigated.

In this work, inspired by [22], [23], [24], [25] and taking into account the complementary advantages of PI and STA, a new varying exponent gain STA is proposed for the grid-connected three-level NPC AFE converter. This method mainly focusses on the exponent gains of the STA, which is different from the idea of latest adaptive-gain sliding-mode control using dynamically adapted control gains [26], [27], [28], [29]. In addition, unlike [22], [23], [24], [25], the novel varying exponent gain STA proposed in this article is a combination of the PI controller and the STA by dynamically adjusting the exponent gain α between 1 and 0.5, which keeps the features of PI control (smooth control input) and STA (robustness and fast dynamic response) simultaneously. The adaptive law of the exponent gain α designed in this work requires fewer tuning parameters compared to [25], which facilitates its implementation in actual applications. In addition, it should be pointed out that the control gains (not the exponent gain) used in [22], [23], [24], and [25] are constant, which indicates that the control gains used in both controllers (e.g., linear state feedback control and twisting control) are the same during the switching. However, in actual applications, to achieve the best performance with two controllers using the same control gains is not easy, e.g., small control gains are required for PI to ensure smooth control whereas large control gains are required for STA to assure strong robustness and fast dynamic response when subject to large disturbances. In this sense, the performance of the controllers proposed in [22], [23], [24], and [25] is limited to some extent. In this work, this issue has been addressed by using a set of time-varying control gains related to parameter α. Note that, unlike the adaptive-gain STA introduced in [19], [20], and [21], the control gains designed in proposed method are dynamically adapted based on the exponent coefficient α and will not increase the tuning burden of the proposal from the actual implementation point of view. In the sequel, the best performance of the PI control (smooth control input) and STA (robustness and fast dynamic response) can be achieved simultaneously with the proposed varying exponent gain STA. The dc link is a crucial component of the AFE converter, and its voltage should remain constant in steady state. However, the unknown external disturbances, such as the active power impact generated by the dc loads and RESs, may induce fluctuations of the dc-link voltage and damage the operation of the system. Although the sliding-mode control provides strong robustness regarding the disturbances, extremely high control gains are required if the disturbances are too large, which will generate unacceptable chattering phenomenon. In general, this issue can be addressed effectively by introducing the disturbance observation techniques, and the disturbance observer-based sliding-mode control strategies have been recently proposed in many publications [30]. In [31], a linear extended state observer (LESO)-based STA is applied to the three-level NPC AFE converter to reject external disturbances. In [32], LESO-based fuzzy neural network sliding-mode control is proposed for the active power filter to estimate the parameter perturbation and external disturbance. Then, in [33], a reduced-order generalized PI observer-based resonant STA is proposed for the two-level AFE converter to deal with the time-varying

disturbances. In [34], an LESO-based sliding-mode control is proposed for the dc–dc converter to handle mismatched disturbances. Although the aforementioned linear observers provide good performance with respect to disturbances rejection, they only achieve an exponential convergence of the estimation errors (without finite-time convergence). Then, in [35], a second-order sliding-mode observer (SOSMO)-based sliding-mode control is implemented in the two-level AFE converter and the finite-time stability of the observer is assured. However, the convergence rate of this observer is limited when the system trajectories are far away from the origin, i.e., a large power (disturbances) generated abruptly in the dc link of the AFE converter.

To overcome this problem, in this work, a higher order sliding-mode observer (HOSMO) is designed for the three-level NPC AFE converter to assist the varying exponent gain STA to reject external disturbances. Compared to the SOSMO, the HOSMO not only inherits the virtue of finite-time convergence but also ensures a sufficiently fast convergence rate even when the system trajectories are far from the origin.

Consequently, this article proposes a HOSMO-based varying exponent gain STA (HOSMO-VEGSTA) control scheme for the three-level NPC AFE converter, and the main contributions of this work can be summarized by following points.

1) A novel varying exponent gain STA is proposed for the three-level NPC AFE converter. By introducing a time-varying exponent gain α, the proposed controller blends the merits of both PI control (smooth control input) and STA (robustness and fast dynamic response). In addition, several time-varying control gains are designed to assure that the optimal performance of both controllers are achieved during the switching without extra tuning burden.
2) A HOSMO is designed for the three-level NPC AFE converter in conjunction with the varying exponent gain STA, which further improves the ability of the system to reject external unknown disturbances.

In order to facilitate the practical implementation of the proposed method in actual applications, the tuning procedures of the varying exponent gain STA are also provided in this article. In addition, a series of comparative experiments among PI, HOSMO-based PI (HOSMO-PI), HOSMO-based STA (HOSMO-STA), and the proposed method are carried out based on the three-level NPC AFE prototype, which verifies the superiority of the proposed method.

II. System Model

The three-phase three-level NPC AFE converter is composed of three inductors, two capacitors and numerous power semiconductors, as shown in Fig. 1. On the dc side, a variety of devices may be connected to the dc link, such as dc loads, RESs, and other power converters according to different application scenarios. Generally, they can be regarded as external disturbances since the active power impact may be generated by these devices. In this article, the active power impact is presented by connecting the dc loads.

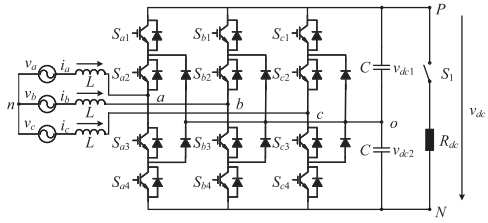

Fig. 1. Topology of three-level NPC AFE converter.

Suppose that the three-phase ac voltages are balanced and the power losses in the converter are neglected, then the system model of the converter in $\alpha\beta\gamma$ coordinate frame can be deduced as [36]

$$L\frac{di_{\alpha\beta}}{dt} = v_{\alpha\beta} - \frac{v_{\rm dc}}{2}\delta_{\alpha\beta} + \frac{e_{\rm dc}}{\sqrt{3}}\begin{bmatrix}\frac{\sqrt{2}(\delta_\beta^2-\delta_\alpha^2)}{4} - \delta_\alpha\delta_\gamma \\ \frac{1}{\sqrt{2}}\delta_\alpha\delta_\beta - \delta_\beta\delta_\gamma\end{bmatrix} \tag{1}$$

$$C\frac{dv_{\rm dc}}{dt} = \delta_{\alpha\beta}^T i_{\alpha\beta} - \frac{2v_{\rm dc}}{R_{\rm dc}} \tag{2}$$

$$C\frac{de_{\rm dc}}{dt} = \frac{1}{\sqrt{6}}\left(i_\alpha\delta_\alpha^2 - i_\alpha\delta_\beta^2 - 2i_\beta\delta_\alpha\delta_\beta\right) + \frac{2\delta_{\alpha\beta}^T i_{\alpha\beta}\delta_\gamma}{\sqrt{3}}. \tag{3}$$

Remark 1: The capacitor voltages must be balanced if the NPC converter is operated correctly, i.e., $e_{\rm dc}$ is close to zero or at least much less than $v_{\rm dc}$. Thus, the inductor currents dynamics given in (1) can be approximated as (4)

$$L\frac{di_{\alpha\beta}}{dt} = v_{\alpha\beta} - \frac{v_{\rm dc}}{2}\delta_{\alpha\beta}. \tag{4}$$

III. Controller Design

Generally, the control structure of the three-level NPC AFE converter can be categorized into three loops, that is, voltage regulation loop (outer loop), instantaneous power tracking loop (inner loop), and voltage balancing loop. In this work, a HOSMO-VEGSTA control scheme is proposed for the three-level NPC AFE converter, which is introduced as follows.

A. Voltage Regulation Loop

1) Higher Order Sliding-Mode Observer: In this section, a HOSMO is designed for the three-level NPC AFE converter to compensate external disturbances, i.e., the active power impact generated in the dc link. The capacitor voltages dynamics shown in (2) can be rewritten as

$$C\frac{dv_{\rm dc}}{dt} = \frac{2p}{v_{\rm dc}} - \frac{2p_r}{v_{\rm dc}} \tag{5}$$

where p_r is the active power consumed by the dc loads, which is regarded as the external disturbance. Suppose that the dynamic of the inner loop is much faster than the dynamic of the outer loop [37], which implies that the dynamics of the inner loop can be neglected when the outer loop controller is designed, and it can be assumed that $p^* \approx p$. With this consideration, defining a new variable $x_1 = v_{\rm dc}^2/2$, then (5) can be presented as

$$\frac{C}{2}\dot{x}_1 = u_d - x_2, \quad \dot{x}_2 = x_3, \quad \dot{x}_3 = h(t), \quad y = x_1 \tag{6}$$

where $u_d = p^*$ is the control input, $x_2 = p_r$ is the disturbances, i.e., the active power impact in the dc link. x_3 represents the time derivative of the disturbances and y denotes the output of the system. Suppose that x_3 is a Lipschitz, and its time derivative is bounded by a positive constant H, i.e., $|h(t)| \leq H$ and $H > 0$. Defining the estimation errors

$$e = \begin{bmatrix} e_1 \\ e_2 \\ e_3 \end{bmatrix} = \begin{bmatrix} x_1 - \hat{x}_1 \\ x_2 - \hat{x}_2 \\ x_3 - \hat{x}_3 \end{bmatrix} \tag{7}$$

where $\hat{x}_1$, $\hat{x}_2$, and $\hat{x}_3$ are the estimation values of x_1, x_2, and x_3, respectively. Afterwards, a HOSMO is designed to estimate the disturbances, which can be presented as

$$\begin{aligned} \frac{C}{2}\dot{\hat{x}}_1 &= u_d - \hat{x}_2 + \beta_1 |e_1|^{2/3} \operatorname{sgn}(e_1) \\ \dot{\hat{x}}_2 &= \hat{x}_3 - \beta_2 |e_1|^{1/3} \operatorname{sgn}(e_1) \\ \dot{\hat{x}}_3 &= -\beta_3 \operatorname{sgn}(e_1) \end{aligned} \tag{8}$$

where β_1, β_2, and β_3 are some positive constants. Subtracting (8) from (6) yields the dynamic of the estimation errors

$$\begin{aligned} \frac{C}{2}\dot{e}_1 &= -e_2 - \beta_1 |e_1|^{2/3} \operatorname{sgn}(e_1) \\ \dot{e}_2 &= e_3 + \beta_2 |e_1|^{1/3} \operatorname{sgn}(e_1) \\ \dot{e}_3 &= \beta_3 \operatorname{sgn}(e_1) + h(t). \end{aligned} \tag{9}$$

It is noteworthy that (9) can be rewritten as normalized form

$$\begin{aligned} \dot{z}_1 &= z_2 - \beta_1 \left(\frac{2}{C}\right)^{2/3} |z_1|^{2/3} \operatorname{sgn}(z_1) \\ \dot{z}_2 &= z_3 - \beta_2 \left(\frac{2}{C}\right)^{1/3} |z_1|^{1/3} \operatorname{sgn}(z_1) \\ \dot{z}_3 &= -\beta_3 \operatorname{sgn}(z_1) + h_{\text{op}}(t) \end{aligned} \tag{10}$$

where $z_1 = \frac{C}{2}e_1$, $z_2 = -e_2$, $z_3 = -e_3$, $h_{\text{op}}(t) = -h(t)$. The finite-time stability of (10) has been proved in [38] and [39], which implies that the estimation errors e_1, e_2, and e_3 will converge to zero in a finite time $t > T_1 > 0$ with appropriately selected observer gains β_1, β_2, and β_3.

2) Varying Exponent Gain STA: In this part, a new varying exponent gain STA is proposed for the NPC AFE converter to regulate the dc-link voltage. The sliding surface is selected as

$$s_d = x_1^* - x_1 \tag{11}$$

where v_{dc}^* is the reference of dc-link voltage, $x_1^* = {v_{\text{dc}}^*}^2/2$. In general, the reference of the dc-link voltage v_{dc}^* is a constant value in the NPC converter, which implies that $\dot{x}_1^* = 0$. Therefore, by substituting (6) into (11), the time derivative of the sliding surface can be derived as

$$\dot{s}_d = a_d - b_d u_d \tag{12}$$

where $a_d = 2x_2/C$ and $b_d = 2/C$.

Remark 2: In consideration of system (12), there exists a variety of sliding-mode controllers in to handle with this kind of tracking problem. One promising alternative is the well-known STA, this method only requires the information of sliding variable s_d and has the advantages of robustness to disturbance and fast dynamic response. However, the chattering of this method will be amplified when some high control gains are required in the NPC converter. Therefore, in this work, a modified version of the STA, i.e., the varying exponent gain STA is proposed for the NPC converter, which can combine the advantages of PI controller (smooth control input) and STA (robustness and fast dynamic response) simultaneously, and the basic idea of this method is shown in Fig. 2 .

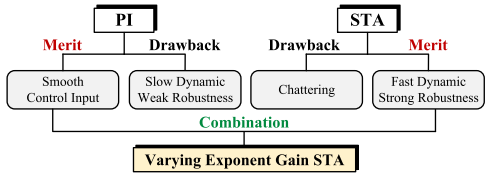

Fig. 2. Basic idea of the proposed varying exponent gain STA.

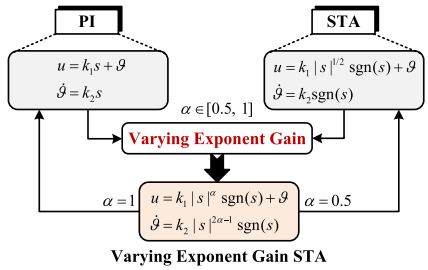

Fig. 3. Schematic diagram of the proposed varying exponent gain STA.

A new varying exponent gain STA can be designed as

$$\begin{aligned} u &= k_1 |s_d|^{\alpha} \operatorname{sgn}(s_d) + \vartheta \\ \dot{\vartheta} &= k_2 |s_d|^{2\alpha-1} \operatorname{sgn}(s_d) \end{aligned} \tag{13}$$

where k_1 and k_2 are the control gains, which are some positive constants. ϑ is an auxiliary variable. α is the exponent gain, which is a time-varying value with $\alpha \in [\frac{1}{2}, 1]$. When $\alpha = \frac{1}{2}$, the varying exponent gain STA becomes a standard STA

$$\begin{aligned} u &= k_1 |s_d|^{1/2} \operatorname{sgn}(s_d) + \vartheta \\ \dot{\vartheta} &= k_2 \operatorname{sgn}(s_d). \end{aligned} \tag{14}$$

On the contrary, the varying exponent gain STA becomes a standard PI controller when $\alpha = 1$

$$\begin{aligned} u &= k_1 s_d + \vartheta \\ \dot{\vartheta} &= k_2 s_d. \end{aligned} \tag{15}$$

Therefore, by designing a time-varying exponent gain α properly, the varying exponent gain STA can smoothly switch between the PI control and the STA and obtain the advantages of both controllers (smooth control input, robustness, and fast dynamic response). Fig. 3 presents the schematic diagram of the proposed varying exponent gain STA.

Remark 3: One has to be fully aware that the control gains k_1 and k_2 are constant in (13) when α is evolving between $\frac{1}{2}$ and 1, which denotes that the control gains of both controllers

are the same during the switching. Nevertheless, it is not easy to achieve the best performance of the PI control and the STA simultaneously only using one set of control gains in actual applications. For instance, the small gains are used in PI controller to achieve smooth control but high gains are required for STA when a large disturbance appears.

In order to address the aforementioned problem, the time-varying control gains are introduced in the varying exponent gain STA, and the controller (13) is redesigned as

$$\begin{aligned} u &= k_1\alpha^m|s_d|^\alpha \operatorname{sgn}(s_d) + \vartheta \\ \dot{\vartheta} &= k_2\alpha^n|s_d|^{2\alpha-1} \operatorname{sgn}(s_d) \end{aligned} \tag{16}$$

where m and n are the negative constants, which means that the control gains $k_1\alpha^m$ and $k_2\alpha^n$ will increase when α varies from 1 (corresponds to PI) to $\frac{1}{2}$ (corresponds to STA). The logic of using the time-varying control gains to achieve the best performance of both controllers is given in Remark 4.

The design of the variation law of the parameter α is the core of the varying exponent gain STA. Therefore, to ensure that the proposed method can correctly switch between PI controller and STA, a rule (variation law) must be set to detect the timing of the switch. That means, a "detector" ε should be constructed in a way that as soon as the sliding variable s_d leaves the domain $[-\varepsilon, \varepsilon]$, the proposed varying exponent gain STA switches to a standard STA, and when the sliding variable are evolving in the domain $|s_d| \leq \varepsilon$, the parameter α should vary between 1 and $\frac{1}{2}$ continuously. In particular, $\alpha = 1$ when $s_d = 0$, so that the proposed varying exponent gain STA can switch to a pure PI controller in this scenario.

Based on the aforementioned discussion, the variation law of parameter α can be designed as

$$\alpha = \max\left(\frac{\varepsilon}{|s_d| + \varepsilon}, \frac{1}{2}\right) \tag{17}$$

where $\varepsilon > 0$ is a positive constant.

Remark 4: Clearly, when $|s_d|$ increases and moves away from the sliding surface, it implies that the robustness of the system is degraded. Hence, the value of α reduces and the values of controller gains $k_1\alpha^m$ and $k_2\alpha^n$ increase based on the variation law (17). Finally, the varying exponent gain STA turns into a standard STA with high gains (strong robustness) forcing the sliding variable $|s_d|$ to the sliding surface rapidly. On the other hand, when the sliding variable $|s_d|$ converges to a small vicinity of the sliding surface, the value of α increases and the values of controller gains $k_1\alpha^m$ and $k_2\alpha^n$ decreases automatically to attenuate the chattering phenomenon. In particular, $\alpha = 1$ when $s_d = 0$, and the varying exponent gain STA turns into a pure PI controller.

3) Higher Order Sliding-Mode Observer-Based Varying Exponent Gain STA: Since the knowledge of the disturbance has been estimated by the HOSMO (see Section III-A), it is necessary to compensate the disturbance and enhance the disturbance rejection ability of the controller. Therefore, the proposed HOSMO-VEGSTA is built as

$$u_d = k_1\alpha^m|s_d|^\alpha \operatorname{sgn}(s_d) + \vartheta_d + \hat{x}_2$$

$$\dot{\vartheta}_d = k_2\alpha^n|s_d|^{2\alpha-1} \operatorname{sgn}(s_d). \tag{18}$$

Direct substitution of (18) into (12) yields

$$\begin{aligned} \dot{s}_d &= -b_d k_1\alpha^m|s_d|^\alpha \operatorname{sgn}(s_d) + \omega_d + e_d \\ \dot{\omega}_d &= -b_d k_2\alpha^n|s_d|^{2\alpha-1} \operatorname{sgn}(s_d) \end{aligned} \tag{19}$$

where $e_d = 2e_2/C$.

Remark 5: It has been proved in Section III-A that the estimation errors e will converge to zero in finite time, which implies that there exists a finite time $T_1 > 0$ such that $e_1 = e_2 = e_3 = 0$ after $t > T_1$. It should be pointed out that system (19) is a practical physical system, which means that all the parameters and physical variables in this system are bounded. Therefore, the states of system (19) cannot escape to infinity in a finite time [40]. In addition, generally, the observer gains are selected such that the estimation errors converge faster than the system trajectories [41]. Therefore, after $t > T_1$, system (19) can be rewritten as

$$\begin{aligned} \dot{s}_d &= -b_d k_1\alpha^m|s_d|^\alpha \operatorname{sgn}(s_d) + \omega_d \\ \dot{\omega}_d &= -b_d k_2\alpha^n|s_d|^{2\alpha-1} \operatorname{sgn}(s_d). \end{aligned} \tag{20}$$

Theorem 1: Considering system (20) and the variation law given in (17), suppose that $k_1 > 0$ and $k_2 > 0$, then there exists some positive constants ζ and ρ such that the system trajectories of (20) converge to a vicinity of zero, i.e., $|s_d| \leq \zeta$, $|\dot{s}_d| \leq \rho$, in a finite time.

Proof: At first, taking into account the case that the sliding variable is far away from the sliding surface and $|s_d| > \varepsilon$, then according to the variation law (17), one has $\alpha = \frac{1}{2}$, and the system dynamic (20) turns into

$$\begin{aligned} \dot{s}_d &= -\lambda_1|s_d|^{1/2} \operatorname{sgn}(s_d) + \omega_d \\ \dot{\omega}_d &= -\lambda_2 \operatorname{sgn}(s_d) \end{aligned} \tag{21}$$

where $\lambda_1 = \frac{b_d k_1}{2^m}$ and $\lambda_2 = \frac{b_d k_2}{2^n}$. The finite-time stability of abovementioned equation has been proved in [42] if $k_1 > 0$ and $k_2 > 0$, which implies that s_d will keep converging until reaching the domain $|s_d| \leq \varepsilon$.

Once $|s_d| \leq \varepsilon$, the parameter α starts varying between $\frac{1}{2}$ and 1 on the basis of the variation law (17), and the sliding variable are evolving in the domain $|s_d| \leq \varepsilon$. Note that, the value of the parameter α increases while $|s_d|$ decreases and the chattering is attenuated in the meantime. Considering the condition that the sliding surface reaches the boundary of the domain $|s_d| \leq \varepsilon$ again, i.e., $|s_d| = \varepsilon$, at this moment, $\alpha = \frac{1}{2}$, and the dynamic of the sliding variable s_d becomes (21) again, which implies that the finite-time stability is satisfied again, and the system trajectories will converge to the domain $|s_d| \leq \varepsilon$ again in finite time. Hence, it is guaranteed that the system trajectories will always stays in a domain $|s_d| \leq \zeta$, where $\zeta > \varepsilon$ is a positive constant.

Next, the convergence domain of $|\dot{s}_d|$ is discussed. Suppose that the sliding variable s_d enters into the domain $|s_d| \leq \zeta$ with $s_d = \zeta > 0$ at t_1 and keeps inside of it. In this condition, there are two cases to be discussed.

C1. $0 < s_d \leq \zeta$. Since s_d enters into the domain with $s_d = \zeta > \varepsilon > 0$ at t_1, according to (20), $\dot{s}_d$ can be indicated as (22) at

this moment

$$\dot{s}_d = -b_d k_1 (1/2)^m |\zeta|^{1/2} + \omega_{dt_1} \tag{22}$$

where ω_{dt_1} denotes the value of the function ω_d at t_1.

Taking into account (20) again, since $s_d > 0$, it can be deduced that $\dot{\omega}_d < 0$ and ω_d decreases from ω_{dt_1} continuously. Once ω_d is sufficiently small such that $\omega_d < 0$, then it must can be obtained that $\dot{s}_d < 0$ and s_d reduces continuously. As a consequence, since s_d is bounded by ζ, the value of s_d will reduce to 0 in finite time. Clearly, ω_d cannot decrease to infinity in that finite time, which implies that $|\omega_d|$ is bounded.

When $s_d = 0$, one has $\dot{s}_d = \omega_d$, and $\dot{s}_d$ may be positive, negative, or equal to zero. If $\dot{s}_d = 0$, then s_d will stay at the origin; if $\dot{s}_d > 0$, then $s_d > 0$ and C1 case holds, while s_d will reduce to 0 in finite time again; if $\dot{s}_d < 0$ then $s_d < 0$, which will be discussed in next case. Note that, as long as $s_d \in [0, \zeta]$, there always exists a positive constant W_1 such that $|\omega_d| \leq W_1$, and then

$$|\dot{s}_d| \leq b_d k_1 \left(\frac{1}{2}\right)^m \xi + W_1 = \rho_1 \tag{23}$$

where $\xi = \max(1,\ \zeta)$.

C2. $-\zeta \leq s_d < 0$. When $s_d < 0$, it can be obtained that $\dot{\omega}_d > 0$ and ω_d increases from ω_{d0} continuously, where ω_{d0} is the value of the function ω_d when s_d enters into the domain $s_d \in [-\zeta, 0)$ from $s_d = 0$ ($|\omega_{d0}| \leq W_1$ according to C1). Once ω_d is sufficiently large such that $\omega_d > 0$, then it can be deduced that $\dot{s}_d > 0$ and s_d increases continuously. Finally, the value of s_d will increase to 0 in finite time. Clearly, ω_d cannot increase to infinity in that finite time, which implies that $|\omega_d|$ is bounded.

When $s_d = 0$, $\dot{s}_d$ may be positive, negative, or equal to zero. If $\dot{s}_d = 0$, then s_d will stay at the origin; if $\dot{s}_d < 0$, then $s_d < 0$ and C2 case holds, while s_d will increase to 0 in finite time again; if $\dot{s}_d > 0$ then $s_d > 0$ and the condition goes back to C1. It should be noted that as long as $s_d \in [-\zeta, 0]$, there always exists a positive constant W_2 such that $|\omega_d| \leq W_2$, which implies that

$$|\dot{s}_d| \leq b_d k_1 \left(\frac{1}{2}\right)^m \xi + W_2 = \rho_2. \tag{24}$$

The condition that s_d enters into the domain $|s_d| \leq \zeta$ with $s_d = -\zeta < 0$ at t_2 and then always keeps inside of it will not be discussed due to the similar deduction. It is easy to conclude that $|\dot{s}_d| \leq \rho_3$ in this condition, where ρ_3 is a positive constant.

Consequently, combining all the cases and one can obtain

$$|\dot{s}_d| \leq \max(\rho_1,\ \rho_2,\ \rho_3) = \rho \tag{25}$$

where ρ is a positive constant.

Theorem 1 is proven. ■

Remark 6: There are four controller gains in the proposed varying exponent gain STA (k_1, k_2, m, n), and the effect of the selection of controller gains on the stability of the proposed method is analyzed. At first, since the perturbations have been estimated and compensated by HOSMO after $t > T_1$, the finite-time convergence of the sliding variable s_d can be assured when $|s_d| > \varepsilon$ as long as k_1 and k_2 are selected as some positive constants. In addition, the behavior of the proposed varying exponent gain STA is close to that of a PI controller

$$\begin{aligned} u &= k_1 s_d + \vartheta \\ \dot{\vartheta} &= k_2 s_d \end{aligned} \tag{26}$$

in steady state, thus, the steady-state performance of the system depends on the selection of controller gains k_1, k_2. Therefore, k_1, k_2 should be properly selected based on frequency domain analysis to assure the stability and performance of the system in steady state. The detailed frequency domain analysis of PI controller from controller gain selection (k_1 and k_2) point of view can be found in [43].

Second, since $\alpha \in [\frac{1}{2}, 1]$, one can obtain that $\alpha^m > 0$ and $\alpha^n > 0$ regardless of the selection of the gains m and n. Therefore, the finite-time convergence of the sliding variable s_d can be assured when $|s_d| > \varepsilon$ whatever the controller gains m and n are chosen. However, the controller gains m and n are related to the performance of the proposed method when it smoothly switches between PI controller and STA, which should be selected properly. The detailed tuning method of these two parameters will be given in Remark 8.

Remark 7: It should be pointed out that although the proposed varying exponent gain STA combines the attractive features of PI controller (smooth control input) and STA (robustness and fast dynamic response) simultaneously, it requires more parameters compared with these two approaches, which increases the implementation complexity of the proposed method in practical engineering applications. Therefore, in order to further facilitate its implementation in practical engineering applications, the tuning procedures of this method are also introduced, which are given in Remark 8.

Remark 8: The tuning procedures of the varying exponent gain STA are introduced as follows.

1) $k_1 > 0$ and $k_2 > 0$ are some constant parameters, they can be directly selected as the control gains of the PI controller when optimal performance is obtained. The PI controller is tuned based on the frequency domain analysis approach [43] and expert method [44]. First, the approximate range of the gains of PI controller are obtained by frequency domain analysis method, and the detailed analysis process can be found in [43]. Then, an expert method given in [44] is used to obtain the optimal gain values. This approach tests the behavior of each transient response and the corresponding control gains, thus, a tuning map can be directly extracted. Finally, the parameters of the PI controller can be obtained according to the desired characteristic based on the tuning map. Afterwards, the parameters k_1 and k_2 can be directly chosen as the control gains of the PI controller because $\alpha^m = 1$ and $\alpha^n = 1$ when the varying exponent gain STA turns into a PI controller ($\alpha = 1$) according to (16). In this sense, the proposed varying exponent gain STA can achieve the desired performance of the PI controller when $\alpha = 1$.
2) m and n are the constant parameters. According to (16), the proposed varying exponent gain STA turns into a STA

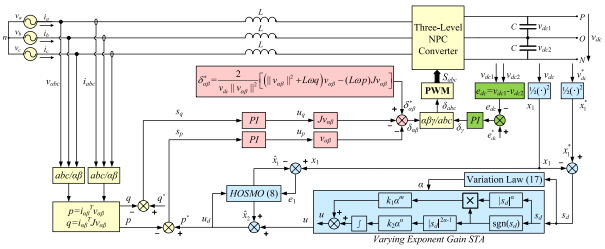

Fig. 4. Control block diagram of proposed HOSMO-VEGSTA control scheme for the three-level NPC AFE converter.

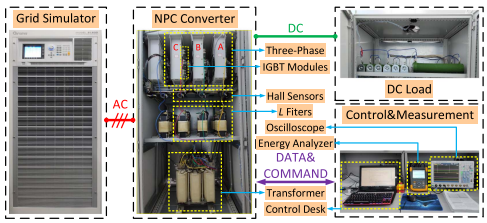

Fig. 5. Laboratory prototype of three-phase NPC converter.

when $\alpha = \frac{1}{2}$, which is presented as

$$u = \frac{k_1}{2^m}|s_d|^{1/2}\,\mathrm{sgn}(s_d) + \vartheta$$
$$\dot{\vartheta} = \frac{k_2}{2^n}\,\mathrm{sgn}(s_d). \tag{27}$$

In order to get the desired performance (robustness and fast dynamic response) of the controller when the proposed varying exponent gain STA turns into an STA, the parameters m and n should be tuned as

$$m = \log_2 \frac{k_1}{\mu_1}, \quad n = \log_2 \frac{k_2}{\mu_2} \tag{28}$$

where μ_1 and μ_2 are the control gains of the STA achieving desired performance. The tuning procedure of the STA applied to the three-level NPC converter can be found in [17]. As a consequence, by introducing the functions α^m and α^n, the control gains become some time-varying values, thus, the desired performance of the PI control and the STA can be both achieved by using the proposed varying exponent gain STA.

3) $\varepsilon > 0$ is a constant parameter. This parameter is related to the accuracy of the controller. Reducing ε will improve the accuracy of the system while the average value of α is also decreased, which induces more chattering. Therefore, the parameter ε is finally determined based on the required tradeoff between accuracy and chattering.

The control structure of this loop is shown in Fig. 4 (the part highlighted in blue).

Remark 9: It should be noticed that the proposed varying exponent gain STA is a general solution and is not only applicable to the three-level NPC converter but also to a variety of power converters. Since the proposed varying exponent gain STA is a combination of PI and STA so that this method can be also extended to apply in a variety of power converters that PI and STA could be used, such as the two-level converters and the dc–dc converters.

TABLE I
SYSTEM PARAMETERS

Description	Parameters	Values	Unites
AC voltage	v_{abc}	230	V_{rms}
Line inductor	L	2	mH
DC-link capacitor	C	6000	μF
Reference of dc voltage	v^*_{dc}	750	V
Reference of reactive power	q^*	0	kvar
Grid frequency	f	50	Hz
Switching frequency	f_{sw}	6.4	kHz

B. Instantaneous Power Tracking Loop

The control objective of this loop is to constrain the active and reactive powers to track their references. The active power p and reactive power q can be presented as

$$p = i^T_{\alpha\beta} v_{\alpha\beta}$$
$$q = i^T_{\alpha\beta} J v_{\alpha\beta}, \quad J = \begin{bmatrix} 0 & -1 \\ 1 & 0 \end{bmatrix}. \tag{29}$$

According to the system model (2)–(4), the time derivative of the active and reactive powers can be deduced as

$$\dot{p} = \frac{v^T_{\alpha\beta}}{L}\left(v_{\alpha\beta} - \frac{v_{dc}}{2}\delta_{\alpha\beta}\right) + \omega q$$
$$\dot{q} = -\frac{v_{dc}}{2L}\delta^T_{\alpha\beta} J v_{\alpha\beta} - \omega p. \tag{30}$$

In this work, the output regulation subspaces-based direct power control reported in [36] is utilized in the inner loop. When the system operates correctly in steady state, the values of the active and reactive power should track their reference values and maintain constant, that is, $\dot{p} = 0$ and $\dot{q} = 0$. In this sense, (30) can be solved as

$$\delta^*_{\alpha\beta} = \frac{2}{v_{dc}\left\|v_{\alpha\beta}\right\|^2}\left[\left(\left\|v_{\alpha\beta}\right\|^2 + L\omega q\right) v_{\alpha\beta} - (L\omega p) J v_{\alpha\beta}\right] \tag{31}$$

where $\delta^*_{\alpha\beta}$ is the average duty cycle when the system correctly operates in steady state, which is also called equilibrium point. In order to force the system trajectories to the equilibrium point, the actual output average duty cycle is presented as (details can be found in [36])

$$\delta_{\alpha\beta} = \delta^*_{\alpha\beta} - u_p v_{\alpha\beta} - u_q J v_{\alpha\beta} \tag{32}$$

where u_p and u_q are the control inputs of the active power and reactive power, respectively. The tracking errors of the active power s_p and reactive power s_q are defined as

$$s_p = p^* - p, \quad s_q = q^* - q. \tag{33}$$

Then, for simplicity purpose, two PI controllers are used to achieve the target of power tracking, which are designed as

$$u_j = k_{pj} s_j + k_{ij} \int_0^t s_j d\tau, \quad j = p, q \tag{34}$$

TABLE II
PARAMETERS OF DIFFERENT CONTROLLERS

Controller	Power tracking loop	Voltage regulation loop	Voltage balancing loop
PI	$k_{pp} = k_{pq}$ = 9e−8 $k_{ip} = k_{iq}$ = 1e−7	k_{pv} = 0.1 k_{iv} = 2	k_{pb} = 5e−3 k_{ib} = 1e−5
HOSMO-PI	$k_{pp} = k_{pq}$ = 9e−8 $k_{ip} = k_{iq}$ = 1e−7	k_{pv} = 0.1, k_{iv} = 2 β_1 = 20, β_2 = 1e4, β_3 = 1e5	k_{pb} = 5e−3 k_{ib} = 1e−5
HOSMO-STA	$k_{pp} = k_{pq}$ = 9e−8 $k_{ip} = k_{iq}$ = 1e−7	μ_1 = 12.8, μ_2 = 64 β_1 = 20, β_2 = 1e4, β_3 = 1e5	k_{pb} = 5e−3 k_{ib} = 1e−5
HOSMO-VEGSTA	$k_{pp} = k_{pq}$ = 9e−8 $k_{ip} = k_{iq}$ = 1e−7	k_1 = 0.1, k_2 = 2, m = -7, n = -5, ε = 2500 β_1 = 20, β_2 = 1e4, β_3 = 1e5	k_{pb} = 5e−3 k_{ib} = 1e−5

where k_{pj}, k_{ij} are the gains of PI controllers. The structure of this loop is shown in Fig. 4 (the part highlighted in pink).

C. Voltage Balancing Loop

In this loop, the target is to guarantee the voltage balancing of the two capacitors in dc link. Given the assumption that the dynamics of the active and reactive powers are much faster than the dynamics of the capacitors voltages in dc link [37], which implies that the instantaneous powers operate at the equilibrium point when the voltage balancing control strategy is designed. In this case, introducing (31) in (3) yields

$$\dot{e}_{\rm dc} = \frac{4p^*}{\sqrt{3}v_{\rm dc}C}\delta_\gamma + \psi(t) \tag{35}$$

where $\psi(t) = \frac{1}{\sqrt{6}C}\left[(\delta_\alpha^*)^2 i_\alpha - (\delta_\beta^*)^2 i_\alpha - 2\delta_\alpha^*\delta_\beta^* i_\beta\right]$.

Similar as the instantaneous power tracking loop, an effective PI controller is designed for this loop to assure the voltage balancing, which is presented as

$$\delta_\gamma = k_{pb}e_d + k_{ib}\int_0^t e_d d\tau \tag{36}$$

where k_{pb} and k_{ib} are the control gains of the PI controller, $e_d = e_{\rm dc}^* - e_{\rm dc}$, $e_{\rm dc}^*$ is the reference of error between capacitors voltages and in general $e_{\rm dc}^* = 0$. The control structure of this loop is shown in Fig. 4 (the part highlighted in green).

IV. EXPERIMENTAL VERIFICATION

For the sake of evaluating the performance of the proposed control scheme, a set of comparative experiments have been carried out among PI, HOSMO-PI, HOSMO-STA, and proposed HOSMO-VEGSTA based on a laboratory test bench, i.e., a grid-connected three-level NPC AFE converter, whose configuration is shown in Fig. 5. The specifications of the converter are listed in Table I, where $V_{\rm rms}$ denotes the root-mean-square (RMS) value of the ac voltage. The controllers are executed based on a TMS320F28377D digital signal processor with a predetermined sampling frequency $f_s = 6.4$ kHz. The output control signal is modulated by a basic pulsewidth modulation gate drive, and the switching frequency is fixed, which is set as $f_{\rm sw} = 6.4$ kHz. The control parameters of these controllers are shown in Table II.

To ensure fair comparisons, all the controllers are tuned to obtain good behavior and high performance. The tuning of the PI controller is based on the frequency domain analysis approach [43] and the expert method [44]; the tuning rules of the HOSMO are given in [45]; the tuning of the STA is based on the methodology of error dynamics, and the details can be found in [17], it is tuned such that a sufficiently good robustness and dynamic performance are achieved; the tuning procedures of the VEGSTA are introduced in Remark 8.

A. Comparative Assessment of Dynamic Performance

First, the dynamic performance of different methods is assessed. Fig. 6 shows the dc-link voltage and ac current (phase a) under a voltage step from 690 to 750 V, where $\Delta V_{\rm step}$ is the overshoot voltage and ΔT is the settling time. Fig. 7 shows the transient grid voltage waveforms under the same step at $t = 0.4$ s. As it can be seen, compared to the conventional PI controller, the HOSMO-STA provides a faster dynamic response. This advantage is captured by the proposed HOSMO-VEGSTA by using varying exponent gain, which lies in the almost identical dynamic performance as HOSMO-STA.

B. Comparative Assessment of Disturbance Rejection Ability

Second, the ability to reject perturbations of different controllers is evaluated. At $t = 0.4$ s, a 150 Ω dc load is connected to the dc link of the NPC AFE converter regarded as an external disturbance, and the corresponding dc-link voltage waveforms and current waveforms (phase a) are shown in Fig. 8. It can be seen that the HOSMO-STA and the proposed HOSMO-VEGSTA achieve the same disturbance rejection ability in the presence of a perturbation, which is better than the PI controller. The active and reactive power as well as grid voltage response under such disturbance with different controllers are shown Figs. 9 and 10. Apparently, due to the stronger disturbance rejection ability, the HOSMO-STA and the proposed HOSMO-VEGSTA provide faster dynamic response than the PI controller under an active power step. In addition, the variation of the parameter α under this condition is presented in Fig. 11. Clearly, the value of the parameter α is close to 1 in steady state, which means the behavior of the VEGSTA is close to that of a PI controller, thus a smooth control is ensured and the chattering is attenuated. When the disturbance appears at $t = 0.4$ s, the value of the parameter α decreases to $\frac{1}{2}$ rapidly, and the proposed VEGSTA turns into a standard STA to enhance the robustness of the controller. Finally, the system returns to steady state, and the value of the parameter α varies around 1 again to reduce the chattering.

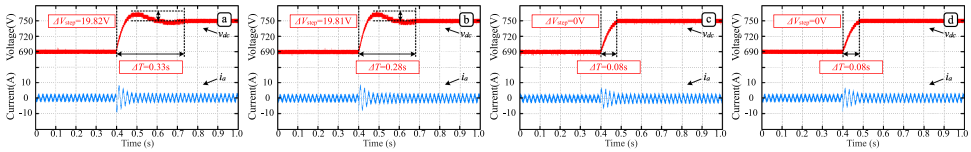

Fig. 6. Transient responses of the DC-link voltage and grid current (phase a) under a step from 690 to 750 V based on different controllers. (a) PI. (b) HOSMO-PI. (c) HOSMO-STA. (d) HOSMO-VEGSTA.

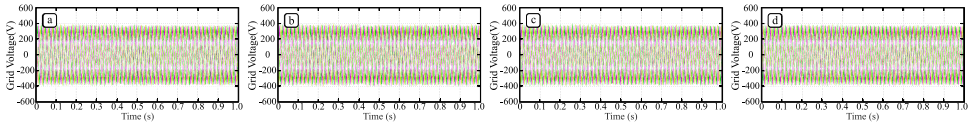

Fig. 7. Transient grid voltage waveforms when NPC converter is subject to a voltage step from 690 to 750 V at $t = 0.4$ s based on different controllers. (a) PI. (b) HOSMO-PI. (c) HOSMO-STA. (d) HOSMO-VEGSTA.

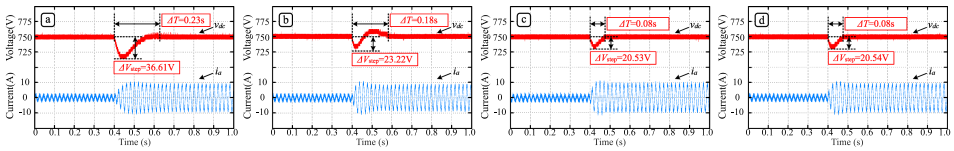

Fig. 8. DC-link voltage and grid current (phase a) under a 150 Ω load step based on different controllers. (a) PI. (b) HOSMO-PI. (c) HOSMO-STA. (d) HOSMO-VEGSTA.

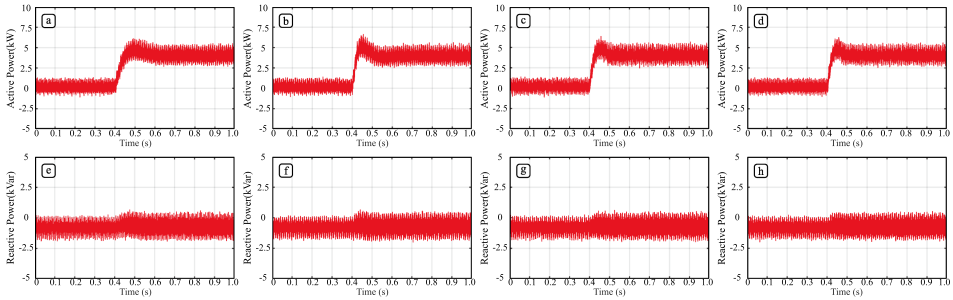

Fig. 9. Active and reactive powers under a 150 Ω load step based on different controllers. Active power: (a) PI. (b) HOSMO-PI. (c) HOSMO-STA. (d) HOSMO-VEGSTA; Reactive power: (e) PI. (f) HOSMO-PI. (g) HOSMO-STA. (h) HOSMO-VEGSTA.

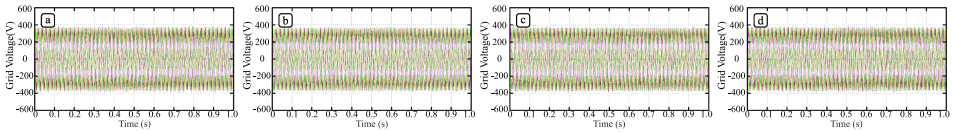

Fig. 10. Transient grid voltage waveforms when NPC converter is subject to a 150 Ω load step at $t = 0.4$ s based on different controllers. (a) PI. (b) HOSMO-PI. (c) HOSMO-STA. (d) HOSMO-VEGSTA.

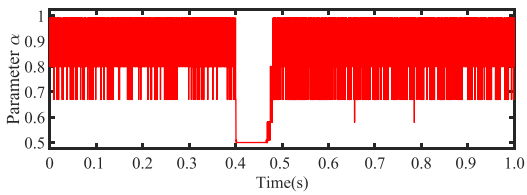

Fig. 11. Parameter α versus time under a 150 Ω load step based on the proposed HOSMO-VEGSTA.

C. Comparative Assessment of Steady-State Performance

Third, the steady-state performances of the NPC AFE converter with different controllers are evaluated. Fig. 12 shows the control input u_d of different controllers when the NPC AFE converter operates in steady state with a 5.3 kW power consumption ($R_1 = 150$ Ω and $R_2 = 360$ Ω are connected to the dc link). Clearly, the control action magnitude of the HOSMO-STA is much larger than others. Since the control input of the voltage regulation loop u_d is also the reference of the active power p^*, thus, the quality of current will be affected

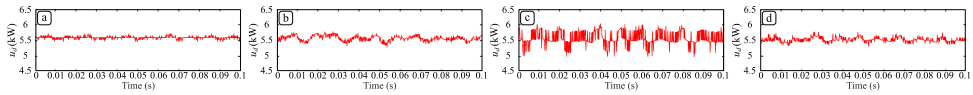

Fig. 12. Control input of the voltage regulation loop of NPC AFE converter in steady state based on different controllers. (a) PI. (b) HOSMO-PI. (c) HOSMO-STA. (d) HOSMO-VEGSTA.

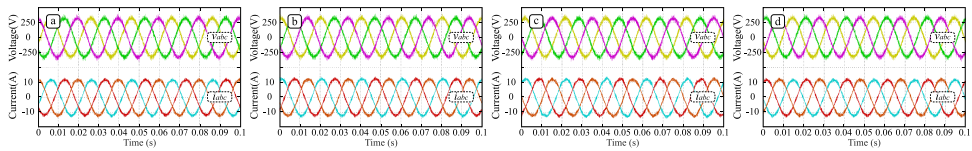

Fig. 13. Three-phase grid voltage and grid current waveforms of the NPC AFE converter in steady state with a 5.3 kW power consumption based on different controllers. (a) PI. (b) HOSMO-PI. (c) HOSMO-STA (d) HOSMO-VEGSTA.

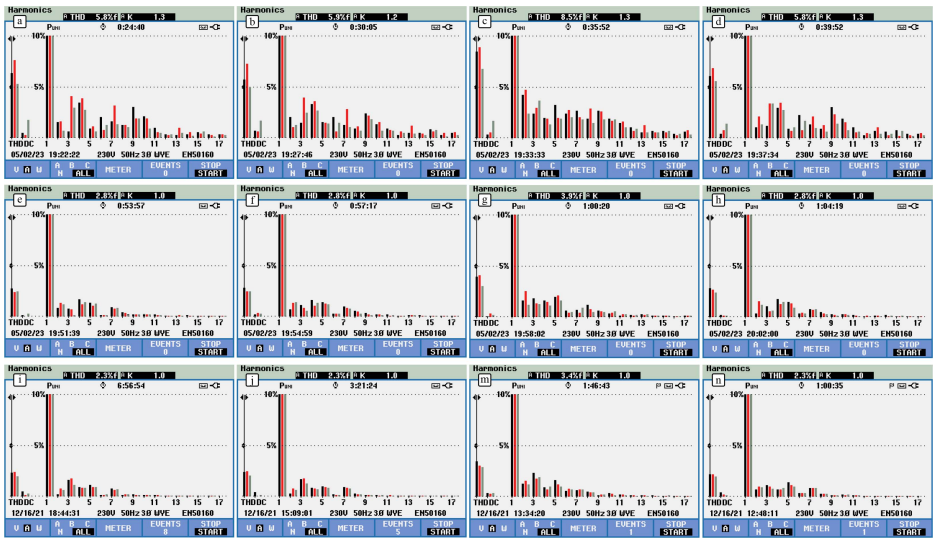

Fig. 14. Three-phase grid currents harmonic spectra of the NPC AFE converter in steady state under different conditions. 1) The unloading condition: (a) PI. (b) HOSMO-PI. (c) HOSMO-STA. (d) HOSMO-VEGSTA. 2) The loading condition with a 3.7 kW power consumption: (e) PI. (f) HOSMO-PI. (g) HOSMO-STA. (h) HOSMO-VEGSTA. 3) The loading condition with a 5.3 kW power consumption: (i) PI. (j) HOSMO-PI. (m) HOSMO-STA. (n) HOSMO-VEGSTA.

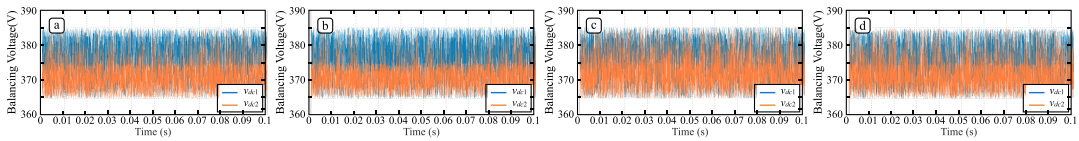

Fig. 15. Balancing voltage (v_{dc1} and v_{dc2}) of the NPC AFE converter in steady state with a 5.3 kW power consumption. (a) PI. (b) HOSMO-PI. (c) HOSMO-STA. (d) HOSMO-VEGSTA.

if a large high-frequency switching control action is generated by the voltage regulation loop. Fig. 13 shows the three-phase grid voltage and grid current waveforms in steady state with a 5.3 kW power consumption, and Fig. 14 presents the ac currents harmonic spectra in steady state under different conditions. It can be seen that the proposed HOSMO-VEGSTA achieves the advantage of the PI controller in steady state, i.e., the similar current quality, which is better than the HOSMO-STA. Fig. 15 shows the balancing voltage (v_{dc1} and v_{dc2}) of the NPC AFE converter in steady state with a 5.3 kW power consumption, and it can been observed that the capacitors voltages in dc link are balanced with each method.

D. Robustness Assessment of Proposed Method Under Parameter Variation

At last, the robustness of the proposed method with respect to parameter uncertainty is assessed. In this scenario, the value of the capacitor C has a +10% variation in the control implementation, and the corresponding dynamic and steady state as well as disturbance rejection performance with the proposed HOSMO-VEGSTA method are presented in Fig. 16, and the observer output of the proposed method under a 150 Ω load step with C variation is given in Fig. 17. It can be seen that the performance of the proposed method keep almost the same under parameter variation, which validates the

TABLE III
PERFORMANCE COMPARISON OF DIFFERENT METHODS

Methods	Dynamic performance (A step from 650 to 750 V)		Disturbances rejection performance (A 150 Ω load step)		Steady state performance (Under 5.3 kW power consumption)
	Overshoot voltage (V)	Settling time (s)	Voltage Sag (V)	Settling time (s)	Current THD value (%)
PI	19.82	0.33	36.61	0.23	**2.3**
HOSMO-PI	19.81	0.28	23.22	0.18	**2.3**
HOSMO-STA	**0**	**0.08**	**20.53**	**0.08**	3.4
HOSMO-VEGSTA	**0**	**0.08**	**20.54**	**0.08**	**2.3**

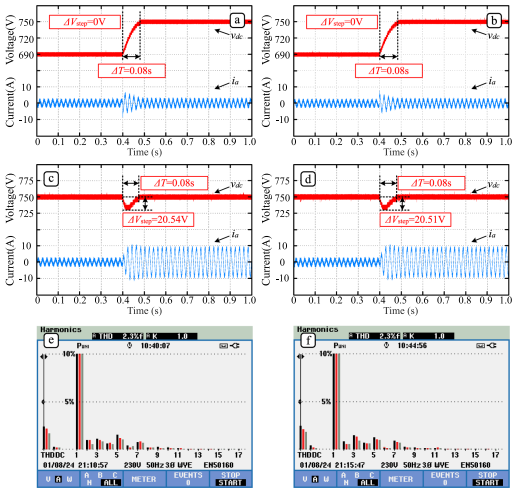

Fig. 16. Dynamic, steady state and disturbance rejection performance of proposed method with and without C variation (+10%). (a) Voltage step (690–750 V). (b) Voltage step (690–750 V) with C variation. (c) 150 Ω load step. (d) 150 Ω load step with C variation. (e) Grid current THD for a 5.3 kW active power consumption. (f) Grid current THD for a 5.3 kW active power consumption with C variation.

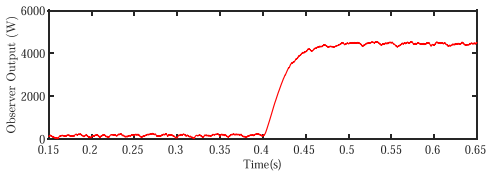

Fig. 17. Observer output of the proposed method under a 150 Ω load step with C variation.

robustness of the proposed method with respect to parameter uncertainty.

Finally, a performance comparison of these methods are presented in Table III to clearly illustrate the advantages of the proposed HOSMO-VEGSTA method compared with the others. The bold values denotes better performance compared with others. Apparently, the proposed HOSMO-VEGSTA contains the features of PI control (smooth control input) and STA (robustness and fast dynamic response) simultaneously.

V. CONCLUSION

In this article, a HOSMO-VEGSTA control scheme is proposed for the three-level NPC AFE converters. To combine the complementary advantages of PI (smooth control input) and STA (robustness and fast dynamic response), a novel varying exponent gain STA is proposed in this work. By designing a time-varying exponent gain α, the proposed controller smoothly switches between PI ($\alpha = 1$) and STA ($\alpha = \frac{1}{2}$), capturing their merits simultaneously. Meanwhile, a HOSMO is designed combining varying exponent gain STA to further enhance the disturbance rejection ability of the converters. As a combinatorial innovation method, the proposed strategy exhibits high performance in both steady state as well as transient and provides strong robustness, thus, the performance of the three-level NPC AFE converters in various applications (such as motor drives, dc microgrids, and RESs) can be further improved compared to conventional PI and STA. The main limitation of the proposed method (increased tuning parameters compared to PI and STA) is also considered, and the detailed tuning procedures of the proposed method are introduced to facilitate its implementation in practical applications. In addition, since the proposed method is a combination of PI and STA, it can also be extended to apply in a variety of power converters where PI and STA could be used, e.g., two-level converters and dc–dc converters. Finally, the proposed method is compared to the standard PI controller and STA using a lab-constructed three-level NPC converter prototype, and the experimental results show that the proposed control scheme achieves smooth control input, strong robustness, and fast dynamic response simultaneously, whose performance is superior to both PI and STA. Future work will focus on investigating the first-order sliding-mode control and higher order sliding-mode control with varying exponent gains, and their application to the power converters.

REFERENCES

[1] S. Haq et al., "A modified PWM scheme to improve the power quality of NPC inverter based solar PV fed induction motor drive for water pumping," *IEEE Trans. Ind. Appl.*, vol. 59, no. 3, pp. 3019–3030, May/Jun. 2023.

[2] T. Dragičević, X. Lu, J. C. Vasquez, and J. M. Guerrero, "DC microgrids-Part II: A review of power architectures, applications, and standardization issues," *IEEE Trans. Power Electron.*, vol. 31, no. 5, pp. 3528–3549, May 2016.

[3] K. Kumari and A. K. Jain, "Performance assessment of three-phase NPC-based grid integrated single-stage solar PV system with reduced DC bus capacitor," *IEEE Trans. Ind. Electron.*, vol. 70, no. 4, pp. 3773–3781, Apr. 2023.

[4] W. Xu, M. M. Ismail, and M. R. Islam, *Permanent Magnet Synchronous Machines and Drives: Flux Weakening Advanced Control Techniques*. Boca Raton, FL, USA: CRC Press, 2023, doi: 10.1201/9781003320128.

[5] J. Yang, H. Cui, S. Li, and A. Zolotas, "Optimized active disturbance rejection control for DC-DC buck converters with uncertainties using a reduced-order GPI observer," *IEEE Trans. Circuits Syst. I: Regular Papers*, vol. 65, no. 2, pp. 832–841, Feb. 2018.

[6] T. Dragičević, S. Vazquez, and P. Wheeler, "Advanced control methods for power converters in DG systems and microgrids," *IEEE Trans. Ind. Electron.*, vol. 68, no. 7, pp. 5847–5862, Jul. 2021.

[7] X. Shen et al., "Adaptive second-order sliding mode control for grid-connected NPC converters with enhanced disturbance rejection," *IEEE Trans. Power Electron.*, vol. 37, no. 1, pp. 206–220, Jan. 2022.
[8] Y. Gui, F. Blaabjerg, X. Wang, J. D. Bendtsen, D. Yang, and J. Stoustrup, "Improved dc-link voltage regulation strategy for grid-connected converters," *IEEE Trans. Ind. Electron.*, vol. 68, no. 6, pp. 4977–4987, Jun. 2021.
[9] L. Wu, J. Liu, S. Vazquez, and S. K. Mazumder, "Sliding mode control in power converters and drives: A review," *IEEE/CAA J. Automatica Sinica*, vol. 9, no. 3, pp. 392–406, Mar. 2022.
[10] L. Guo, N. Jin, Y. Li, and K. Luo, "A model predictive control method for grid-connected power converters without AC voltage sensors," *IEEE Trans. Ind. Electron.*, vol. 68, no. 2, pp. 1299–1310, Feb. 2021.
[11] S. Wang, T. Dragicevic, Y. Gao, S. K. Chaudhary, and R. Teodorescu, "Machine learning based operating region extension of modular multilevel converters under unbalanced grid faults," *IEEE Trans. Ind. Electron.*, vol. 68, no. 5, pp. 4554–4560, May 2021.
[12] S. Vazquez et al., "Model predictive control: A review of its applications in power electronics," *IEEE Ind. Electron. Mag.*, vol. 8, no. 1, pp. 16–31, Mar. 2014.
[13] X. Shen et al., "Adaptive-gain second-order sliding mode control of NPC converters via super-twisting technique," *IEEE Trans. Power Electron.*, vol. 38, no. 12, pp. 15406–15418, Dec. 2023.
[14] Z. Liu et al., "A novel faster fixed-time adaptive control for robotic systems with input saturation," *IEEE Trans. Ind. Electron.*, vol. 71, no. 5, pp. 5215–5223, May 2024.
[15] Z. Ma, Z. Liu, P. Huang, and Z. Kuang, "Adaptive fractional-order sliding mode control for admittance-based telerobotic system with optimized order and force estimation," *IEEE Trans. Ind. Electron.*, vol. 69, no. 5, pp. 5165–5174, May 2022.
[16] L. Liu et al., "A robust high-quality current control with fast convergence for three-level NPC converters in micro-energy systems," *IEEE Trans. Ind. Informat.*, vol. 19, no. 11, pp. 10716–10726, Nov. 2023.
[17] J. Liu et al., "Sliding mode control of grid-connected npc converters via high-gain observer," *IEEE Trans. Ind. Electron.*, vol. 69, no. 4, pp. 4010–4021, Apr. 2022.
[18] Y. Yin et al., "Observer-based sliding mode control for grid-connected power converters under unbalanced grid conditions," *IEEE Trans. Ind. Electron.*, vol. 69, no. 1, pp. 517–527, Jan. 2022.
[19] Y. Shtessel, M. Taleb, and F. Plestan, "A novel adaptive-gain supertwisting sliding mode controller: Methodology and application," *Automatica*, vol. 48, no. 5, pp. 759–769, May 2012.
[20] T. Gonzalez, J. A. Moreno, and L. Fridman, "Variable gain super-twisting sliding mode control," *IEEE Trans. Autom. Control*, vol. 57, no. 8, pp. 2100–2105, Aug. 2012.
[21] V. I. Utkin and A. S. Poznyak, "Adaptive sliding mode control with application to super-twist algorithm: Equivalent control method," *Automatica*, vol. 49, no. 1, pp. 39–47, Jan. 2013.
[22] E. Tahoumi, M. Ghanes, F. Plestan, and J.-P. Barbot, "A new controller switching between linear and twisting algorithms," in *Proc. Annu. Amer. Control Conf.*, 2018, pp. 6150–6155.
[23] E. Tahoumi, F. Plestan, M. Ghanes, and J.-P. Barbot, "A controller switching between twisting and linear algorithms for an electropneumatic actuator," in *Proc. Eur. Control Conf.*, 2018, pp. 2368–2373.
[24] E. Tahoumi, F. Plestan, M. Ghanes, and J.-P. Barbot, "Adaptive exponent parameter: A robust control solution balancing between linear and twisting controllers," in *Proc. 15th Int. Workshop Variable Struct. Syst.*, 2018, pp. 186–191.
[25] E. Tahoumi, F. Plestan, M. Ghanes, and J.-P. Barbot, "New robust control schemes based on both linear and sliding mode approaches: Design and application to an electropneumatic actuator," *IEEE Trans. Control Syst. Technol.*, vol. 29, no. 2, pp. 818–825, Mar. 2021.
[26] J. L. Anderson, J. J. Moré, P. F. Puleston, and R. Costa-Castelló, "Fuel cell module control based on switched/time-based adaptive super-twisting algorithm: Design and experimental validation," *IEEE Trans. Control Syst. Technol.*, vol. 31, no. 1, pp. 434–441, Jan. 2023.
[27] L. Chen, H. Zhang, H. Wang, K. Shao, G. Wang, and A. Yazdani, "Continuous adaptive fast terminal sliding mode-based speed regulation control of PMSM drive via improved super- twisting observer," *IEEE Trans. Ind. Electron.*, vol. 71, no. 5, pp. 5105–5115, May 2024.
[28] D. Jin, L. Liu, Q. Lin, and D. Liang, "Sensorless control strategy of PMSM with disturbance rejection based on adaptive sliding mode control law," *IEEE Trans. Transport. Electrific.*, to be published, doi: 10.1109/TTE.2023.3327144.
[29] J. Park, W. Kwon, and P. Park, "An improved adaptive sliding mode control based on time-delay control for robot manipulators," *IEEE Trans. Ind. Electron.*, vol. 70, no. 10, pp. 10363–10373, Oct. 2023.
[30] P. A. Hosseinabadi, H. Pota, S. Mekhilef, and H. Schwartz, "Fixed-time observer-based control of DFIG-based wind energy conversion systems for maximum power extraction," *Int. J. Elect. Power Energy Syst.*, vol. 146, 2023, Art. no. 108741.
[31] X. Shen et al., "High-performance second-order sliding mode control for NPC converters," *IEEE Trans. Ind. Informat.*, vol. 16, no. 8, pp. 5345–5356, Aug. 2020.
[32] J. Wang and J. Fei, "Self-feedback neural network sliding mode control with extended state observer for active power filter," *IEEE Internet Things J.*, vol. 10, no. 13, pp. 11724–11738, Jul. 2023.
[33] J. Lu, M. Savaghebi, A. M. Y. Mohammad Ghias, X. Hou, and J. M. Guerrero, "A reduced-order generalized proportional integral observer-based resonant super-twisting sliding mode control for grid-connected power converters," *IEEE Trans. Ind. Electron.*, vol. 68, no. 7, pp. 5897–5908, Jul. 2021.
[34] J. Linares-Flores et al., "Sliding mode control based on linear extended state observer for dc-to-dc buck-boost power converter system with mismatched disturbances," *IEEE Trans. Ind. Appl.*, vol. 58, no. 1, pp. 940–950, Jan./Feb. 2022.
[35] W. Luo, S. Vazquez, J. Liu, F. Gordillo, L. G. Franquelo, and L. Wu, "Control system design of a three-phase active front end using a sliding-mode observer," *IEEE Trans. Syst., Man, Cybern. Syst.*, vol. 52, no. 2, pp. 739–748, Feb. 2022.
[36] R. Portillo, S. Vazquez, J. I. Leon, M. M. Prats, and L. G. Franquelo, "Model based adaptive direct power control for three-level NPC converters," *IEEE Trans. Ind. Informat.*, vol. 9, no. 2, pp. 1148–1157, May 2013.
[37] F. Umbría, J. Aracil, F. Gordillo, F. Salas, and J. A. Sánchez, "Three-time-scale singular perturbation stability analysis of three-phase power converters," *Asian J. Control*, vol. 16, no. 5, pp. 1361–1372, 2014.
[38] M. T. Angulo, J. A. Moreno, and L. Fridman, "Robust exact uniformly convergent arbitrary order differentiator," *Automatica*, vol. 49, no. 8, pp. 2489–2495, 2013.
[39] J. A. Moreno, "Lyapunov function for levant's second order differentiator," in *Proc. IEEE 51st Conf. Decis. Control*, 2012, pp. 6448–6453.
[40] J. A. Moreno, "A Lyapunov approach to output feedback control using second-order sliding modes," *IMA J. Math. Control Inf.*, vol. 29, no. 3, pp. 291–308, 2012.
[41] A. Chalanga, S. Kamal, L. M. Fridman, B. Bandyopadhyay, and J. A. Moreno, "Implementation of super-twisting control: Super-twisting and higher order sliding-mode observer-based approaches," *IEEE Trans. Ind. Electron.*, vol. 63, no. 6, pp. 3677–3685, Jun. 2016.
[42] J. A. Moreno and M. Osorio, "A lyapunov approach to second-order sliding mode controllers and observers," in *Proc. 47th IEEE Conf. Decis. Control*, 2008, pp. 2856–2861.
[43] H. Lin et al., "Integral sliding-mode control-based direct power control for three-level NPC converters," *Energies*, vol. 13, no. 1, p. 227, 2020. [Online]. Available: https://mdpi.longhoe.net/1996-1073/13/1/227
[44] J. Litt, "An expert system to perform on-line controller tuning," *IEEE Control Syst. Mag.*, vol. 11, no. 3, pp. 18–23, Apr. 1991.
[45] A. Levant, "Higher-order sliding modes, differentiation and output-feedback control," *Int. J. Control*, vol. 76, no. 9/10, pp. 924–941, 2003.

Xiaoning Shen (Member, IEEE) received the M.S. degree in electrical engineering from the Harbin Institute of Technology, Shenzhen, China, in 2017 and the Ph.D. degree in control science and engineering from the Harbin Institute of Technology, Harbin, China, in 2022.

Since 2022, he has been an Assistant Professor with the Harbin Institute of Technology, Harbin, China. His current research interests include sliding-mode control, observation methods, and their applications to power electronic systems.

Jianxing Liu (Senior Member, IEEE) received the B.S. degree in mechanical engineering and the M.E. degree in control science and engineering from the Harbin Institute of Technology, Harbin, China, in 2004 and 2010, respectively, and the Ph.D. degree in automation from the Technical University of Belfort-Montbeliard, Belfort, France, in 2014.

He is currently a Professor with the Department of Control Science and Engineering, Harbin Institute of Technology. His current research interests include sliding mode control, nonlinear control and observation, industrial electronics, and renewable energy solutions.

Dr. Liu is currently an Associate Editor for several journals, including IEEE/CAA JOURNAL OF AUTOMATICA SINICA, IEEE TRANSACTIONS CIRCUITS AND SYSTEMS II: EXPRESS BRIEFS, IEEE SYSTEMS JOURNAL, NONLINEAR DYNAMICS, *ISA Transactions*, and IEEE JOURNAL OF EMERGING AND SELECTED TOPICS IN INDUSTRIAL ELECTRONICS. He is also an Associate Editor of the Conference Editorial Board, IEEE Control Systems Society.

Zhuang Liu (Graduate Student Member, IEEE) received the B.S. degree in electrical engineering and automation in 2017 from the China University of Mining and Technology, Xuzhou, China, and the M.E. degree in electrical engineering in 2019 from the Harbin Institute of Technology, Harbin, China, where he is currently working toward the Ph.D. degree in control science and engineering.

His current research interests include adaptive control, sliding-mode control, neural network control, fuzzy logic system, model predictive control, finite-time control, fixed-time control, and their applications to robotics and power electronic systems.

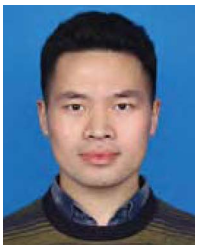

Yabin Gao (Member, IEEE) received the B.M. degree in information management and information systems in 2012, the M.E. degree in software engineering in 2015, both from Bohai University, Jinzhou, China, and the Ph.D. degree in control science and engineering from the Harbin Institute of Technology, Harbin, China, in 2020.

From 2017 to 2019, he was a Visiting Scholar with the Department of Mechanical Engineering, University of Victoria, Victoria, BC, Canada. He is currently an Associate Professor with the Department of Control Science and Engineering, Harbin Institute of Technology. His current research interests include cyber-physical systems, multiagent systems, reliable and safe/secure control, intelligent control, and their applications.

Jose I. Leon (Fellow, IEEE) was born in Cadiz, Spain. He received the B.S., M.S., and Ph.D. degrees in telecommunications engineering from the Universidad de Sevilla, Seville, Spain, in 1999, 2001, and 2006, respectively.

He is currently an Associate Professor with the Universidad de Sevilla with ENGREEN, Seville, Spain. Since 2019, he has also been a Chair Professor with the Harbin Institute of Technology, Harbin, China. His research interests include modulation and control of power converters for high-power applications and renewable energy systems.

Dr. Leon was a corecipient of the 2008, 2015, 2020, and 2022 Best Paper Award of *IEEE Industrial Electronics Magazine*, and the 2012 Best Paper Award of the IEEE TRANSACTIONS ON INDUSTRIAL ELECTRONICS. He was the recipient of the 2014 IEEE J. David Irwin Industrial Electronics Society Early Career Award, the 2017 IEEE Bimal K. Bose Energy Systems Award and the 2017 Manuel Losada Villasante Award.

Sergio Vazquez (Fellow, IEEE) was born in Seville, Spain, in 1974. He received the M.S. and Ph.D. degrees in industrial engineering from the University of Seville (US), Seville, Spain, in 2006 and 2010, respectively.

Since 2002, he has been with the Power Electronics Group working in R&D projects. He is currently an Associate Professor with the Department of Electronic Engineering, US. His research interests include power electronics systems, modeling, modulation, and control of power electronics converters applied to renewable energy technologies.

Dr. Vazquez was recipient as coauthor of the 2012 Best Paper Award of IEEE TRANSACTIONS ON INDUSTRIAL ELECTRONICS and 2015 Best Paper Award of the *IEEE Industrial Electronics Magazine*. He is involved in the Energy Storage Technical Committee of the IEEE Industrial Electronics Society and is currently an Associate Editor for IEEE TRANSACTIONS ON INDUSTRIAL ELECTRONICS.

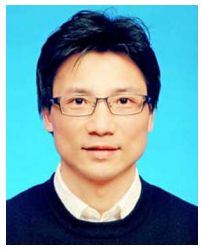

Ligang Wu (Fellow, IEEE) received the B.S. degree in automation, the M.E. degree in navigation guidance and control, and the Ph.D. degree in control theory and control engineering from the Harbin Institute of Technology, Harbin, China, in 2001, 2003, and 2006, respectively.

From 2006 to 2007, he was a Research Associate with the Department of Mechanical Engineering, The University of Hong Kong, Hong Kong. From September 2007 to June 2008, he was a Senior Research Associate with the Department of Mathematics, City University of Hong Kong, Hong Kong. From December 2012 to December 2013, he was a Research Associate with the Department of Electrical and Electronic Engineering, Imperial College London, London, U.K. In 2008, he joined the Harbin Institute of Technology, as an Associate Professor, and was then promoted to a Full Professor in 2012. He has authored or coauthored seven research monographs and more than 170 research papers in international referred journals. His current research interests include switched systems, stochastic systems, computational and intelligent systems, sliding-mode control, and advanced control techniques for power electronic systems.

Dr. Wu was the recipient of the National Science Fund for Distinguished Young Scholars in 2015 and the China Young Five Four Medal in 2016. He was named as the Distinguished Professor of Chang Jiang Scholar in 2017 and the Highly Cited Researcher since 2015. He is currently an Associate Editor for a number of journals, including IEEE TRANSACTIONS ON AUTOMATIC CONTROL, IEEE TRANSACTIONS ON INDUSTRIAL ELECTRONICS, IEEE/ASME TRANSACTIONS ON MECHATRONICS, *Information Sciences*, *Signal Processing*, and *IET Control Theory and Applications*. He is also an Associate Editor for the Conference Editorial Board, IEEE Control Systems Society.

Leopoldo G. Franquelo (Life Fellow, IEEE) was born in Malaga, Spain. He received the M.Sc. and Ph.D. degrees in electrical engineering from the Universidad de Sevilla, Seville, Spain, in 1977 and 1980, respectively.

From 1982 to 1986, he was an Associate Professor with the Electronics Engineering Department, Sevilla University, Seville, Spain, and has been a Professor with the Electronics Engineering Department, Sevilla University since 1986 and a Professor with the Department of Control Science and Engineering, Harbin Institute of Technology since 2016. He has participated in more than 100 Industrial and R&D projects and has published more than 300 papers, 108 of them in IEEE Journals and 25 of them in IEEE Magazines. His current research interests include modulation techniques for multilevel inverters and application to power electronic systems for renewable energy systems.

Dr. Franquelo is currently an IEEE Industrial Electronics Society (IES) Distinguished Lecturer since 2006. In IEEE TRANSACTIONS INDUSTRIAL ELECTRONICS, he became an Associate Editor in 2007, Co-Editor-in-Chief in 2014, and an Editor-in-Chief 2016–2018. He is currently an Editor-in-Chief for the IEEE Open Journal of the Industrial Electronics Society. He was a Member-at-Large of the IES AdCom (2002–2003), Vice President for Conferences (2004–2007), and President Elect of the IES (2008–2009). He was the President of the IES (2010–2011) and is an IES AdCom Life member. In 2009 and 2013, he was the recipient of the prestigious Andalusian Research Award and FAMA Award recognizing the excellence of his research career and a number of Best Paper Awards from IEEE journals. In 2012 and 2015, he was also the recipient of the Eugene Mittelmann Outstanding Research Achievement Award and the Antohny J. Hornfeck Service Award from IEEE-IES, respectively.